Editors' Suggestion

Laser-frequency stabilization using light shift in compact atomic clocks

Claudio E. Calosso, Michele Gozzelino,* Filippo Levi, and Salvatore Micalizio
Istituto Nazionale di Ricerca Metrologica, INRIM, Quantum Metrology and Nanotechnologies Division, Strada delle Cacce 91, Torino 10135, Italy

(Received 28 May 2024; revised 9 August 2024; accepted 22 August 2024; published 12 September 2024)

This paper describes the light-shift laser-lock (LSLL) technique, an alternative method intended for laser-based compact atomic clocks. The technique greatly simplifies the laser setup by stabilizing the pumping-laser frequency to the same atoms involved in the clock operation, without the need of an external reference. By alternating two clock sequences, the method estimates and cancels out a controlled amount of induced light shift, acting on the laser frequency. The LSLL technique is compatible with state-of-the-art three-level clocks and was demonstrated with field-programmable-gate-array-based electronics on a pulsed-optically-pumped vapor-cell clock developed at INRIM. The results have shown that the LSLL technique operates robustly, having a capture range of gigahertz without significantly compromising clock stability. In our tests, the clock exhibited a white frequency noise of $3.2 \times 10^{-13}\tau^{-1/2}$ for averaging times τ up to 4000 s, reaching a floor below 1×10^{-14} up to 100 000 s. This level of performance meets the requirements of future global navigation satellite systems on-board clocks, adding the benefits of a reduced clock footprint, as well as increased reliability and robustness.

DOI: 10.1103/PhysRevApplied.22.034033

I. INTRODUCTION

Laser stabilization is a key tool in atomic and molecular physics experiments, and in particular in atomic clocks [1–3]. Often, the frequency reference is a high-finesse Fabry-Perot cavity or an interferometer [4–6]. When the quality factor of the frequency reference is high, the stabilization can also bring line narrowing. However, being based on macroscopic objects, these frequency references can experience drifts and nonstationary behaviors, which may not always be suitable for applications requiring long-term stability or an absolute frequency reference [5]. In such cases, stabilizing the laser frequency to an atomic transition is often the most effective approach [7–10].

In laser-pumped atomic clocks, the laser light is utilized to prepare the atoms in the desired ground state and to read out the atomic states. Active stabilization of the laser frequency is essential in these cases as well, since frequency-dependent light-shift effects can introduce instability to the clock transition [11,12]. The degree of instability induced by light shift depends on the physical principles of the clock, often requiring state-of-the-art laser stabilization [13–15]. This is also the case with coherent-population-trapping (CPT) clocks, where different techniques have been proposed to mitigate light-shift effects [16–19]. Usually, the laser frequency is stabilized on a dedicated external spectroscopy setup. However, adding a dedicated branch for probing an external reference increases the complexity, size, weight of the clock, which is not desirable for real-world applications [20].

In this paper, we turn the concept around and show that actually the light shift can be conveniently exploited to frequency stabilize the laser, leading to the development of a more compact and robust frequency standard. The idea of using the light shift for laser stabilization was proposed a while ago by Arditi and Picqué, who compared two clocks: one with enhanced light shift and another with regular light shift, serving as a reference [21]. Our work demonstrates that a single clock alternating between high and low light-shift modes avoids the need for an external atomic clock. We named this locking technique "light-shift laser lock" (LSLL).

Since the light-shift profile is a dispersive curve whose width is proportional to the linewith of the excited state, it provides a wide capture range in the case of pumping and read-out lasers. This is even more true in the case of additional sources of line broadening, such as buffer-gas dephasing collisions and Doppler broadening [22]. A wide capture range is an appealing feature for automatic relock procedures and unmanned operation. The technique takes advantage of the same atomic sample used in the clock operation, offering a dual benefit. First, the atoms are usually in a very well-controlled environment, especially

*Contact author: m.gozzelino@inrim.it

in terms of electromagnetic fields and temperature, a desirable condition for the best frequency stability in the long term. Second, being the atomic signal already available, the technique can be implemented with minimal modifications to the clock hardware, mainly relying on firmware or software implementation. This peculiarity makes the method suitable for an easy upgrade in existing systems, provided that they are based on a digital architecture.

Undoubtedly, there are close analogies between the (symmetric) autobalanced Ramsey method [16,23] and other advanced protocols that detect and correct for the light-shift effect [17,18]. In fact, in all these cases, the light shift is estimated by alternating low and high light-shift clock sequences. However, while those techniques compensate for the light shift by acting on the microwave synthesizer, leaving the atoms in the same perturbed conditions, this technique directly acts on the laser frequency to minimize its influence, thereby leaving the atomic sample in a less perturbed state.

We implement the LSLL technique in a pulsed-optically-pumped (POP) clock, where we stabilized the pumping laser without the use of an external frequency reference, and demonstrate state-of-the-art clock stability. This is a major step in increasing the robustness of the POP technology, especially for space applications [24].

We also note that the LSLL technique does not need any frequency modulation, further simplifying the laser setup and preserving the frequency-noise characteristics of the free-running laser, avoiding possibly detrimental amplitude modulation and aliasing effects [25]. We point out that all the aforementioned benefits come at the cost of a more complex clock sequence, which can pose a challenge for analog implementations. However, this technique lends itself well to being implemented on a digital platform, such as those described in Ref. [26].

II. TECHNIQUE

The operation of many compact clocks involves a three-level structure as the one sketched in Fig. 1(a). The clock transition $\nu_{21} = \nu_2 - \nu_1$ lies between two ground states $|1\rangle$ and $|2\rangle$ and a third state is used to perform optical pumping, thus creating a population imbalance [11]. The presence of the optical field generates a frequency shift on the two clock states [27]. With the laser resonant with one of the two ground states, we can approximate the light shift on the clock transition as

$$\Delta\nu_{21} \simeq \frac{(-1)^k}{4} \frac{\Delta\nu_{\mathrm{PL}}}{\Delta\nu_{\mathrm{PL}}^2 + (\Gamma/2)^2} \Omega_{k3}^2, \tag{1}$$

where $\Delta\nu_{\mathrm{PL}} = \nu_{\mathrm{PL}} - \nu_{k3}$ is the pumping-laser (PL) detuning from the atomic transition linking the ground state $|k\rangle$ (either 1 or 2) to the excited state $|3\rangle$ and $\Omega_{k3} = \langle k| \mathbf{d} \cdot \mathbf{E} |3\rangle / h$ is the associated Rabi frequency for the dipole moment $\mathbf{d}$ and the laser field vector $\mathbf{E}$. Γ is the relaxation rate of the level $|3\rangle$. The former expression is valid in the weak coupling limit ($\Omega_{k3} \ll \Gamma$) and neglects atomic motion. When the atomic velocity cannot be neglected, such as in room-temperature atomic vapors, an average over the the velocity distribution must be performed, leading to an additional source of broadening of the light-shift profile [28]. The following features are relevant for the present discussion: close to resonance, the light shift is linear with respect to the laser detuning; the magnitude of the shift is proportional to the square of the Rabi frequency and thus to the intensity of the perturbing laser (I_{PL}); finally, the width of the dispersive curve is proportional to the relaxation rate Γ.

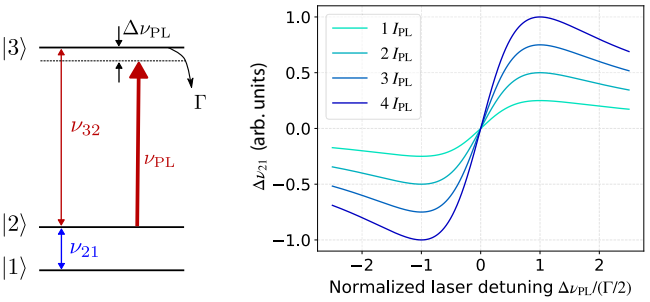

FIG. 1. Left: simplified three-level scheme common to clocks based on ground-state splitting. $\Delta\nu_{\mathrm{PL}}$ is the laser frequency detuning from the transition linking one of the two ground states to the excited state. Γ is the relaxation rate of the excited state. Right: qualitative light shift affecting the clock transition ($\Delta\nu_{21}$) when the laser is nearly resonant with one of the two clock states. This curve can be used as a discriminator for laser stabilization and the laser intensity (I_{PL}, see text) is a free parameter that can be adjusted to optimize the discriminator sensitivity.

Generally, at resonance ($\Delta\nu_{\mathrm{PL}} \ll \Gamma$), the clock frequency is characterized by a sensitivity to the pumping laser frequency expressed as $\beta = \Delta y / \Delta\nu_{\mathrm{PL}}$, where y is the clock fractional frequency fluctuation. The contribution to the clock instability will be therefore $\sigma_y(\tau) = \beta\, \sigma_{\nu_{\mathrm{PL}}}(\tau)$, where τ is the averaging time.

A common method to maintain the laser in resonance and reduce the conversion of laser-frequency fluctuations to clock-frequency fluctuations is to stabilize the frequency of the pumping laser to an external reference. Alternatively, we can consider using the dispersive curve of the light shift as a frequency discriminator for this stabilization, as long as we have a suitable method for directly measuring the light shift. Experimentally, this is done by alternating two clock sequences: "Seq. 1" for which the light-shift is minimal, and "Seq. 2" in which the effect is enhanced by inducing a controlled light shift, for example, by sending an appropriate amount of light during the probing of the clock transition (see Fig. 2).

The error signals of the two clock sequences depend, although to different extents, on both the local oscillator

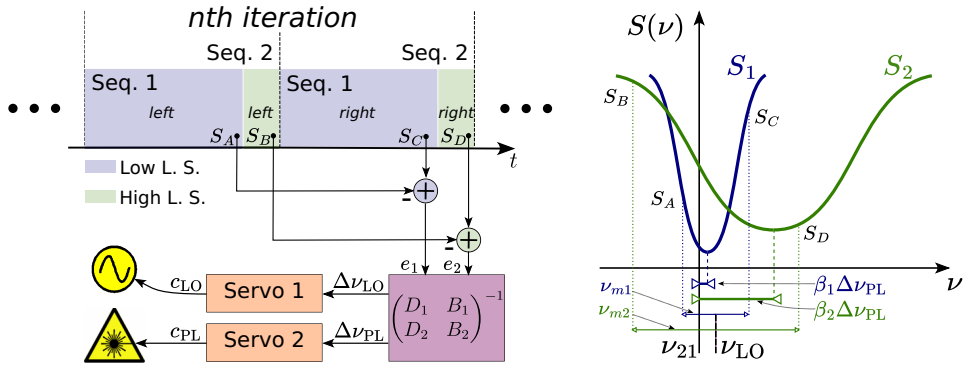

FIG. 2. On the left, the operation principle of the LSLL technique: the four atomic signals are employed to compute the error signals of the two sequences, which depend on both LO and PL detunings. The latter can be retrieved thanks to the inverse of the sensitivity matrix and utilized by dedicated servos to correct both the LO and PL frequencies. On the right, it can be observed how the spectroscopies, which are related to the two sequences, are differently affected by light shift, which is in turn proportional to the laser detuning. Additionally, the LO interrogation frequency is shown with their respective modulations that result in the four atomic signals used by the technique. By enabling the servos, the interrogating LO and the two curves align themselves with the unperturbed frequency, as aligning the PL cancels both light shifts.

(LO) frequency and the pumping laser (PL) frequency, as reported in the following equation:

$$\begin{pmatrix} e_1 \\ e_2 \end{pmatrix} = \begin{pmatrix} D_1 & B_1 \\ D_2 & B_2 \end{pmatrix} \begin{pmatrix} \Delta\nu_{LO} \\ \Delta\nu_{PL} \end{pmatrix} \tag{2}$$

where $\Delta\nu_{LO} = \nu_{LO} - \nu_{21}$ is the detuning of the LO frequency ν_{LO} from the atomic transition frequency estimated with the first clock loop (ν_{21}) and $\Delta\nu_{PL}$ the detuning of the laser frequency ν_{PL} with respect to the frequency ν_{32}. The coefficients B_i are of course proportional to β, whereas D_i are inversely proportional to the atomic quality factor of the clock transition in the two clock sequences. B_2 can be purposely magnified by setting a controlled amount of laser intensity I_{PL} during the clock interrogation of sequence 2.

By inverting the 2×2 matrix presented in Eq. (2), both $\Delta\nu_{LO}$ and $\Delta\nu_{PL}$ can be directly obtained and fed to two dedicated controllers that calculate the corrections c_{LO} and c_{PL} for the LO and PL frequencies, respectively. $\Delta\nu_{LO}$ is used, as usual, to stabilize the LO frequency, while $\Delta\nu_{PL}$, can be utilized for the direct stabilization of the laser frequency to the clock cell, that is the goal of this work.

It is interesting to note that $\Delta\nu_{LO}$ is the error of the local oscillator already corrected for the light shift, showing significant analogies with Ref. [18]. This would suggest that the stabilization of the pumping laser is not strictly required, at least from a theoretical point of view. However, such stabilization is necessary due to the limited precision in the knowledge of the coefficients, their variation in time and with the experimental conditions, and the fact that Eq. (2) represents a first-order approximation. By stabilizing the laser frequency, the light-shift correction is enforced, and the contribution of the second-order terms remains constant, thereby preserving the clock stability.

It is worth noting that both parameters are stabilized using information derived from the same atoms involved in the clock operation. This is achieved through a more complex clock sequence and the ability to process and extract information in real time, requiring significant and dedicated processing capability. In some cases, the information processing can be simplified by bypassing the matrix-inversion step. Specifically, when $(B_1/D_1) \ll (B_2/D_2)$, e_1 can be directly used to stabilize the LO frequency, effectively reducing $\Delta\nu_{LO}$ close to zero. In such conditions, e_2 becomes almost exclusively dependent on the pumping-laser frequency error and can be used directly for its stabilization, thereby bringing the frequency error close to zero and further aligning the LO with the unperturbed atomic frequency ν_{21}. By iterating this process, in steady state, the LO and the PL will tend to ν_{21} and ν_{32}, respectively. However, it is worthwhile to note that, in this context, the sequence 2 is perceived as a dead time, leading to an increase in the Dick effect that requires careful evaluation and management [29,30]. In the experimental demonstration presented in Sec. III, we will indeed operate within this simplified regime. This approach streamlines the implementation without adversely affecting clock performance, as we will demonstrate that the Dick effect remains negligible.

III. IMPLEMENTATION AND RESULTS

The technique detailed in Sec. II was implemented and verified in a rubidium POP clock. The clock setup has been extensively described in Refs. [20,31] for what concerns recent results and in Refs. [26,32] for what concerns the

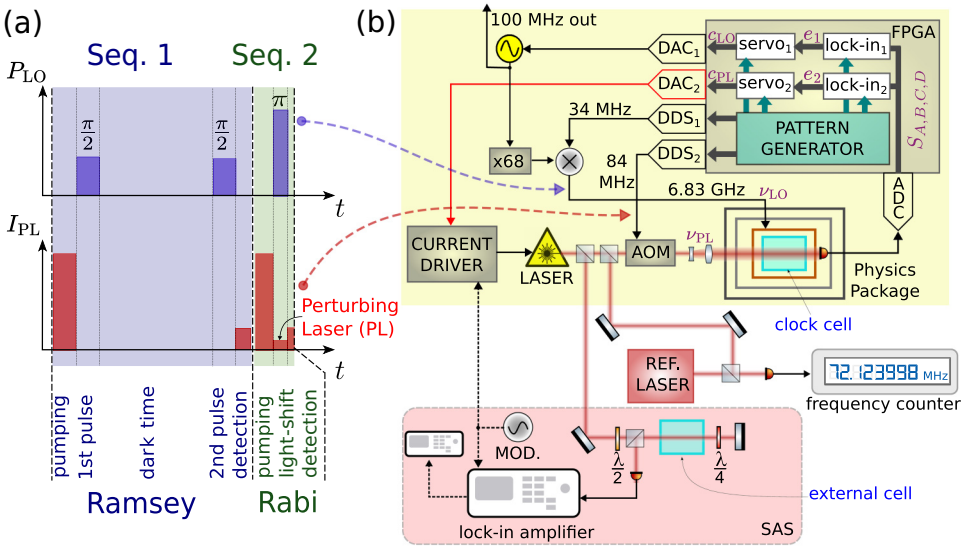

FIG. 3. Implementation of the LSLL technique in a pulsed optically pumped clock: (a) Ramsey and Rabi sequences with related steps. (b) Yellow box: the clock setup consists of the FPGA-based electronics package at the top and the optics and physics packages at the bottom. The laser frequency is locked to the clock cell and then compared to an external reference laser for its frequency measurement and to the external cell, no longer being necessary, serving as a monitor to display the signal obtained with saturated absorption spectroscopy setup, for comparison (red box).

field-programmable-gate-array- (FPGA) based electronics framework. Here, we show in Fig. 3 a simplified diagram of the experimental setup, along with a brief description of it.

Atoms are prepared using a DFB laser, which is pulsed by means of an acousto-optic modulator (AOM). The atomic sample is then interrogated using a microwave signal, which is derived from an ultrastable oscillator. The atomic signal is obtained detecting the transmission of a weak laser pulse with a photodiode and acquiring it with a FPGA through an analog-to-digital converter (ADC).

The clock's pulsed operation is ensured by an embedded pattern generator, which manages the signal processing, as well as the amplitude and frequency modulations of the direct digital synthesizers (DDSs). The DDSs allow us to modulate both the microwave and the laser. The laser frequency is monitored using an external buffer-gas-free cell, through saturated absorption spectroscopy (SAS), and with an optical beatnote with an external reference laser. The clock is, in turn, measured with respect to an active hydrogen maser, which has better stability and frequency drift compared to the clock under test.

In this setup, the LSLL technique stabilizes the laser by processing the atomic signal and acting on the driving current of the laser diode. The atomic signal is processed by two digital lock-in amplifiers to obtain the two error signals, e_1 and e_2, which are directly fed into two pure integrative controllers that calculate c_{LO} and c_{PL}, the corrections to be applied to the tuning voltage of the local oscillator (LO) and the laser's supply current through dedicated digital to analog converters (DACs) (see Fig. 3). The inversion of the matrix in Eq. (2) is not implemented, for simplicity [we are indeed in the case $(B_1/D_1) \ll (B_2/D_2)$]. Thanks to the LSLL technique, the laser is maintained automatically in resonance with the $|5^2S_{1/2}\rangle \rightarrow |5^2P_{3/2}\rangle$ transition frequency, shifted by the buffer gas. We perform optical pumping from the $|F_g = 1\rangle$ ground state. Optical dephasing collisions with the buffer gas and Doppler broadening lead to an effective width of the excited state Γ of $\simeq 1$ GHz, much larger than the hyperfine splitting between the $F' = 0, 1, 2$ components of the $5^2P_{3/2}$ state, leading to a single dispersive signal [33]. The AOM rf frequency takes an absolutely arbitrary value. In contrast, in the POP standard operation the AOM frequency must be set at a specific frequency to bridge the frequency difference in the Rb transitions between the external cell (without buffer gas) and the clock cell.

The amplitude of the microwave field is stabilized using the technique detailed in Ref. [34], whereas the laser power is stabilized in the medium-long-term using a low-bandwidth (time constant 0.5 s) digital control, without reducing the fast laser intensity noise that is at the level of -120 dB 1/Hz at 93 Hz, i.e., the clock modulation frequency.

A demonstration of the LSLL technique was already presented in 2017 [26]. There, the low light-shift POP configuration was alternated with the high light-shift continuous-wave double resonance (CWDR) one. Although the results were encouraging, the CWDR interrogation consisted of a single step where the atoms simultaneously interacted with laser and microwave, preventing the optimization of all the experimental

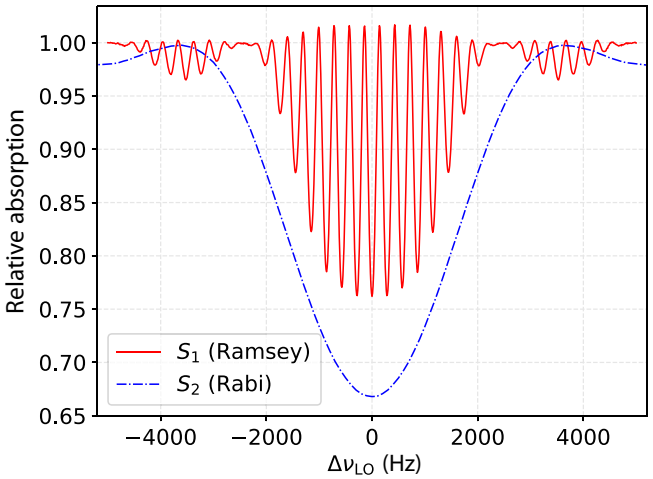

FIG. 4. Red continuous trace: measured absorption signal S_1 as a function of the microwave detuning $\Delta\nu_{LO}$, obtained with the Ramsey sequence ($T = 3$ ms). Blue line-dotted trace: absorption signal S_2 obtained with Rabi sequence (pulse length 0.27 ms).

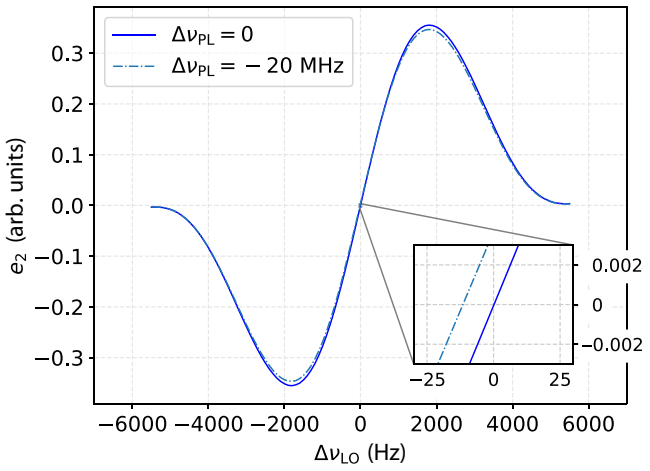

FIG. 5. LSLL error signal e_2 as a function of the local oscillator detuning $\Delta\nu_{LO}$. The inset highlights the light shift induced by the pumping-laser detuning $\Delta\nu_{PL}$. Rabi cycle time = 0.87 ms (pumping time = 0.4 ms, π-pulse = 0.27 ms, $\tau_{d2} = 0.2$ ms). $I_{PL} = 3.5 \times 10^{-2}$ mW cm^{-2}.

parameters. Instead, in this work, we provide a more comprehensive examination of the technique by utilizing the Rabi interrogation. Indeed, the Rabi sequence offers 3 degrees of freedom, enabling independent optimization of atom number, light-shift amount, and detection sensitivity, resulting in more effective and improved outcomes.

As shown in Fig. 3(a), in the present implementation Ramsey and Rabi sequences are alternated. The first one is composed of a short optical pumping pulse ($I = 15$ mW cm^{-2}, duration 0.4 ms), followed by microwave Ramsey sequence (two $\pi/2$ pulses 0.4-ms long, separated by a free-evolution time $T = 3$ ms). Finally, a weak probe pulse ($I = 0.9$ mW cm^{-2}) of duration $\tau_{d1} = 0.3$ ms is sent for measuring the absorption of the atomic vapor. The spectroscopic signal S_1 is obtained by integrating the photodiode signal over τ_{d1}. The signal S_1 measured as a function of the local oscillator (LO) frequency is shown in Fig. 4 (red trace), where we recognize the characteristic Ramsey fringes in the absorption signal. The sequence is repeated twice to enable a square-wave modulation of the microwave around the central Ramsey fringe (modulation depth $\nu_{m1} = 80$ Hz). Following a full modulation cycle, an error signal $e_1 = S_1(\nu_{LO} + \nu_{m1}) - S_1(\nu_{LO} - \nu_{m1}) = S_C - S_A$ is used to perform a bottom-of-the-fringe stabilization of the LO.

The Rabi sequence is composed of a pumping pulse that resets the atomic coherence, i.e., the memory of the atoms, and restores the clock-state population imbalance; then a Rabi pulse is sent, together with a small amount of laser power to induce a controlled amount of light shift on the clock transition; at the end, the $|F_g = 1\rangle$ clock-state population is probed by integrating the absorption signal during an averaging window of length τ_{d2}, obtaining the signal S_2. To keep the dead time of the main clock sequence at a minimum, the Rabi sequence is kept as short as possible (pumping time 0.4 ms, Rabi pulse 0.27 ms, $\tau_{d2} = 0.2$ ms). Pump and probe intensity is the same as in the Ramsey sequence. A typical spectroscopic signal obtained with Seq. 2 is shown in Fig. 4 (line-dotted blue trace). Also in this case, the LO frequency is modulated, now at $\pm\nu_{m2} = \pm 1.8$ kHz, to construct an error signal $e_2 = S_2(\nu_{LO} + \nu_{m2}) - S_2(\nu_{LO} - \nu_{m2}) = S_D - S_B$.

In Fig. 5, we have measured the error signal e_2 as a function of the LO frequency at two different pumping-laser detunings: zero in the blue trace and -20 MHz in the case of the green line-dotted trace. In the inset, we can clearly observe a 11.5 Hz shift, corresponding to a sensitivity $\beta_2 \simeq 8.4 \times 10^{-11}$ MHz^{-2}.

In Fig. 6, the error signal e_2 is plotted as a function of the laser frequency for different intensities of the perturbing laser I_{PL}. As expected, the light-shift scales linearly with the laser intensity, at least for low perturbations, and the discriminant slope increases accordingly. Higher PL intensity increases the signal and makes the system more robust against technical noise and offsets. However, the perturbing light should be kept low enough to limit excess optical pumping and loss of coherence in the clock states. For our experimental apparatus, we found that an intensity I_{PL} in the range of 2×10^{-2} mW cm^{-2} and 4×10^{-2} mW cm^{-2} is a good compromise for having a strong enough signal with minimal perturbation to the system. With $I_{PL} = 3.5 \times 10^{-2}$ mW cm^{-2}, we obtain the following coefficients: $D_1 \simeq 2 \times 10^4$ Hz^{-1}, $B_1 \simeq 0.3$ MHz^{-1}, $D_2 \simeq 2 \times 10^3$ Hz^{-1}, $B_2 \simeq 400$ MHz^{-1}.

In Fig. 6 (lower plot), we also reported for comparison the familiar error signal obtained on a SAS setup, utilizing an isotopically enriched ^{87}Rb cell with no buffer gas. The SAS signal is Doppler-free, leading to much

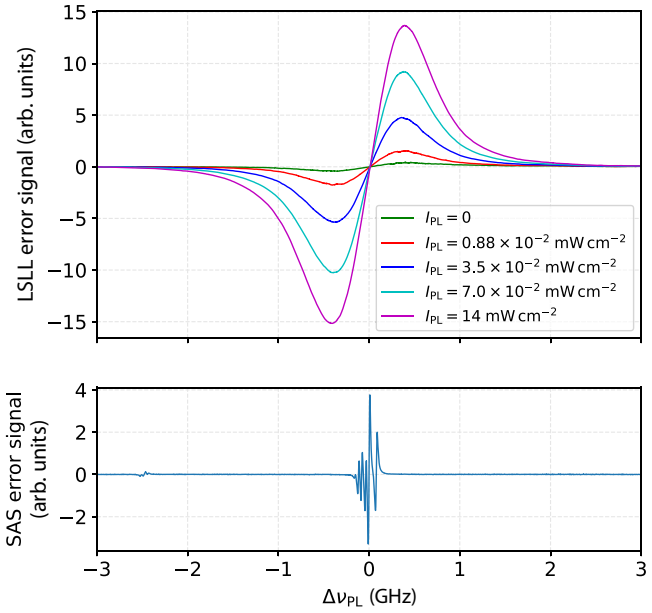

FIG. 6. Upper plot: Error signal e_2 of the interleaved Rabi clock at fixed microwave detuning ($\Delta\nu_{LO} \simeq 0$) as a function of the laser detuning $\Delta\nu_{PL}$. Lower plot: spectroscopy signal obtained in a conventional sub-Doppler saturated absorption setup on an external cell filled with Rb (no buffer gas).

narrower resonances. However, the available signal is typically small, requiring fast modulation and lock-in detection, and the capture range is limited to a few MHz. With the LSLL technique, the error signal has more than 2 GHz capture range and only one resonance, making the stabilization much more robust and appealing for automated clock operation.

A. Laser and clock stabilities

In this section we report the typical laser-frequency stability that we obtained with the LSLL technique. The frequency stability of the laser was evaluated by generating a beatnote with a reference distributed feedback (DFB) laser, which was stabilized using a rubidium cell in a saturated absorption configuration. The resulting beatnote between the two lasers was detected using a fast photodiode (Menlo FPD510) and subsequently measured with a frequency counter (Agilent 53132A) set to a gate time of 1 s (refer to Fig. 3 for details).

In Fig. 7, the free-running stability of our laser diode is reported in terms of Allan deviation (red dots). An upper limit of the frequency stability of the reference laser is reported in green dots. The latter was obtained measuring the frequency stability of two identical SAS setups in a dedicated independent measurement. With blue squares, we report the frequency stability obtained with the LSLL technique. The short-term stability is limited by the detection noise and the locking time constant can be as short

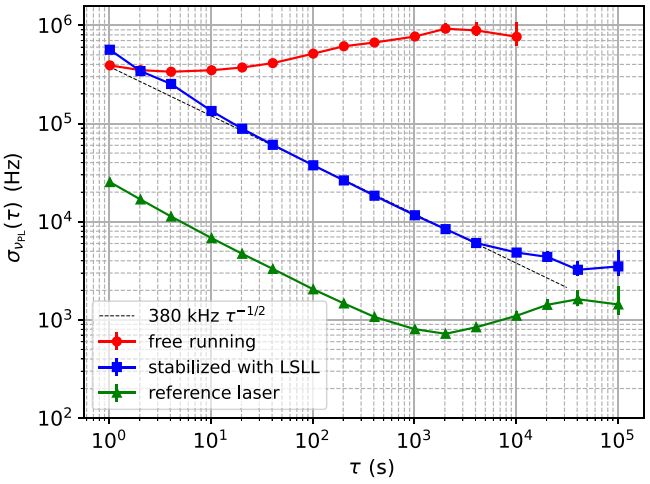

FIG. 7. Typical stability of the DFB laser frequency. Red dots: free-running frequency stability (constant current and constant temperature, no active stabilization). Blue squares: laser stabilized with the LSLL technique. Green triangles: stability of the reference laser used for characterization.

as 100 ms (a few clock cycles). The noise is white up to $\tau = 4000$ s, and reaches 3.5 kHz for an averaging time of one day. This is in line with the results obtained in tabletop spectroscopy setups utilizing much narrower sub-Doppler atomic resonance as a reference. Indeed, for long averaging times the reference laser that we used to perform the measurement has itself a stability of a few kilohertz for daily timescales, and we cannot exclude that it is contributing to the observed instability.

In Fig. 8, we report the typical stability obtained with our POP clock with the laser stabilized on the clock cell with the LSLL method. This stability exhibits white frequency noise of $3.2 \times 10^{-13}\,\tau^{-1/2}$, capable of reaching 1×10^{-14} at 1000 s and maintaining it up to 100 000 s after removing the drift. The technique slightly increases the dead time, from 24.5 % to 36.7 %. However, the Dick effect's short-term impact remains negligible, increasing from $\sigma_y(1\text{ s}) = 2 \times 10^{-14}$ to 3×10^{-14}. We achieved the same short-term stability even without interleaving the second sequence (with the laser stabilized on the external cell), indicating that the observed stability is due to other causes, such as laser intensity noise.

In green, we report the contribution to the clock stability resulting from fluctuations of the laser frequency. This contribution is determined by multiplying the pumping-laser frequency stability, measured synchronously on the beatnote setup against the reference laser, by the clock sensitivity $\beta = -1 \times 10^{-13}\,\text{MHz}^{-1}$. It is evident that the contribution arising from the laser frequency is more than one order of magnitude lower than the measured clock stability. Indeed, the POP clock stability reaches a flicker floor that is consistent with the most recent results obtained with a laser stabilized on a saturated absorption setup [31].

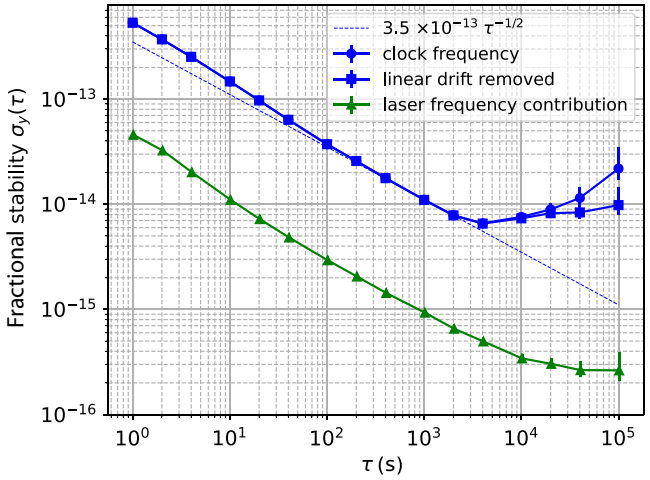

FIG. 8. The stability of the POP clock, obtained using the LSLL technique (blue dots), is shown in terms of Allan deviation. The stability of the clock with a linear drift removed ($2.4\times10^{-14}\,\mathrm{d}^{-1}$) is also depicted with blue squares. The LSLL contribution to the clock stability is shown in green squares, calculated by measuring the laser frequency stability on a dedicated beatnote setup and multiplying it by the sensitivity of the clock ($-1\times10^{-13}\,\mathrm{MHz}^{-1}$).

We would like to emphasize that the LSLL relies on the same atomic signal for the implementation of the LO and PL frequency loops, with the same modulation frequency and similar detection duration. According to Ref. [25], this implies that the detection noise of the LO and the PL frequencies depend on the same portion of the power spectral density, albeit with different sensitivities. Therefore, a variation in the noise characteristics of the atomic signal, for example because a worse laser is used, would lead to a similar variation in the noise contribution on both the LO and PL signals, keeping the relative margin between them unchanged and not compromising the applicability of this technique.

IV. CONCLUSIONS

The proposed light-shift laser-lock technique represents a promising advancement in simplifying the laser setup of compact atomic clocks while mitigating the light-shift effects at the same time. The method is based on a differential measurement, in which a controlled amount of resonant light is purposely introduced on a dedicated interleaved clock sequence. In this way, the shift on the clock transition is probed and used as a discriminator to stabilize the laser frequency.

A major advantage of this scheme lies in avoiding an external reference, as it makes use of the atomic signal already available from the clock interrogation. In this way, the light shift induced by the pump laser is measured and compensated by directly referring to the atoms participating in the clock operation, putting them in a less perturbed state and reducing the effects of light shift on the clock stability. Unlike other methods, LSLL does not require frequency modulation, eliminating a possible additional source of clock instability [35].

This method is particularly promising for laser-pumped vapor-cell clocks, as demonstrated in a Rb POP clock. There, it provides an error signal with a single zero crossing and a capture range exceeding 2 GHz, a feature appealing for industrial uptake of this clock technology [24]. The frequency stability of the laser was below 5 kHz at one-day averaging time, comparable to more conventional laser stabilization techniques based on Doppler-free spectroscopy. With the LSLL, the clock stability reached low 10^{-13} at 1 s, with a floor below 1×10^{-14} up to 100 000 s, a level compliant with the frequency stability specifications of the Galileo second-generation onboard clocks. These results, combined with hardware simplification, make LSLL advantageous for industrial and space applications where compact and robust automatic laser frequency stabilization is highly valued.

Overall, the technique holds potential benefits for miniaturized clocks [36–38], as it requires little or no additional hardware, thus maintaining small size, weight and power consumption while potentially improving long-term frequency stability. Moreover, even if demonstrated on a vapor-cell clock, LSLL is rather general and could be adapted also for other atomic clock technologies involving a three-level system, such as compact microwave ion clocks or even compact optical frequency standards [39,40].

ACKNOWLEDGMENTS

We thank the Atomic Clocks Team of Leonardo S.p.A. and the European Space Agency (ESA) for making the Physics Package Engineering Model "EM2 PP" used for the clock measurements available. EM2 PP is ESA property and it was developed in the frame of the General Support Technology Programme (GSTP), ESA Contract No. 4000118182/16/NL/GLC/FK. We also thank M. Barbiero for careful reading of the manuscript and useful suggestions.

[1] T. N. Bandi, A comprehensive overview of atomic clocks and their applications, Bio., Eng., Med. Sci. Rep. **9**, 1 (2023).

[2] A. D. Ludlow, M. M. Boyd, J. Ye, E. Peik, and P. O. Schmidt, Optical atomic clocks, Rev. Mod. Phys. **87**, 637 (2015).

[3] W. Demtröder, *Laser Spectroscopy: Basic Concepts and Instrumentation* (Springer-Verlag, Berlin Heidelberg New York, 2002).

[4] J. M. Robinson, E. Oelker, W. R. Milner, W. Zhang, T. Legero, D. G. Matei, F. Riehle, U. Sterr, and J. Ye,

Crystalline optical cavity at 4 K with thermal-noise-limited instability and ultralow drift, Optica **6**, 240 (2019).

[5] W. R. Milner, J. M. Robinson, C. J. Kennedy, T. Bothwell, D. Kedar, D. G. Matei, T. Legero, U. Sterr, F. Riehle, H. Leopardi, T. M. Fortier, J. A. Sherman, J. Levine, J. Yao, J. Ye, and E. Oelker, Demonstration of a timescale based on a stable optical carrier, Phys. Rev. Lett. **123**, 173201 (2019).

[6] J. Kong, V. G. Lucivero, R. Jiménez-Martínez, and M. W. Mitchell, Long-term laser frequency stabilization using fiber interferometers, Rev. Sci. Instrum. **86**, 073104 (2015).

[7] T. Preuschoff, M. Schlosser, and G. Birkl, Optimization strategies for modulation transfer spectroscopy applied to laser stabilization, Opt. Express **26**, 24010 (2018).

[8] K. L. Corwin, Z.-T. Lu, C. F. Hand, R. J. Epstein, and C. E. Wieman, Frequency-stabilized diode laser with the Zeeman shift in an atomic vapor, Appl. Opt. **37**, 3295 (1998).

[9] C. Wieman and T. W. Hänsch, Doppler-free laser polarization spectroscopy, Phys. Rev. Lett. **36**, 1170 (1976).

[10] A. Strangfeld, B. Wiegand, J. Kluge, M. Schoch, and M. Krutzik, Compact plug and play optical frequency reference device based on Doppler-free spectroscopy of rubidium vapor, Opt. Express **30**, 12039 (2022).

[11] J. Vanier and C. Audoin, *The Quantum Physics of Atomic Frequency Standards* (Adam Hilger, Bristol, 1989).

[12] J. Vanier and C. Mandache, The passive optically pumped Rb frequency standard: The laser approach, Appl. Phys. B **87**, 565 (2007).

[13] T. Bandi, C. Affolderbach, C. Stefanucci, F. Merli, A. K. Skrivervik, and G. Mileti, Compact high-performance continuous-wave double-resonance rubidium standard with $1.4 \times 10^{-13}\tau^{-1/2}$ stability, IEEE Trans. Ultrason. Ferroelectr. Freq. Control **61**, 1769 (2014).

[14] P. Yun, F. Tricot, C. E. Calosso, S. Micalizio, B. Francois, R. Boudot, S. Guerandel, and E. de Clercq, High-performance coherent population trapping clock with polarization modulation, Phys. Rev. Appl. **7**, 014018 (2017).

[15] B. H. McGuyer, Y.-Y. Jau, and W. Happer, Simple method of light-shift suppression in optical pumping systems, Appl. Phys. Lett. **94**, 251110 (2009).

[16] M. Abdel Hafiz, G. Coget, M. Petersen, C. E. Calosso, S. Guerandel, E. de Clercq, and R. Boudot, Symmetric autobalanced Ramsey interrogation for high-performance coherent-population-trapping vapor-cell atomic clock, Appl. Phys. Lett. **112**, 244102 (2018).

[17] M. Abdel Hafiz, R. Vicarini, N. Passilly, C. E. Calosso, V. Maurice, J. W. Pollock, A. V. Taichenachev, V. I. Yudin, J. Kitching, and R. Boudot, Protocol for light-shift compensation in a continuous-wave microcell atomic clock, Phys. Rev. Appl. **14**, 034015 (2020).

[18] V. I. Yudin, A. V. Taichenachev, M. Y. Basalaev, T. Zanon-Willette, T. E. Mehlstäubler, R. Boudot, J. W. Pollock, M. Shuker, E. A. Donley, and J. Kitching, Combined error signal in Ramsey spectroscopy of clock transitions, New J. Phys. **20**, 123016 (2018).

[19] V. Shah, V. Gerginov, P. D. D. Schwindt, S. Knappe, L. Hollberg, and J. Kitching, Continuous light-shift correction in modulated coherent population trapping clocks, Appl. Phys. Lett. **89**, 151124 (2006).

[20] S. Micalizio, F. Levi, C. E. Calosso, M. Gozzelino, and A. Godone, A pulsed-laser Rb atomic frequency standard for GNSS applications, GPS Solut. **25**, 94 (2021).

[21] M. Arditi and J.-L. Picqué, Application of the light-shift effect to laser frequency stabilization with reference to a microwave frequency standard, Opt. Commun. **15**, 317 (1975).

[22] W. Happer and B. S. Mathur, Effective operator formalism in optical pumping, Phys. Rev. **163**, 12 (1967).

[23] C. Sanner, N. Huntemann, R. Lange, C. Tamm, and E. Peik, Autobalanced Ramsey spectroscopy, Phys. Rev. Lett. **120**, 053602 (2018).

[24] P. Arpesi, J. Belfi, M. Gioia, N. Marzoli, R. Romani, A. Sapia, M. Gozzelino, C. Calosso, F. Levi, S. Micalizio, A. Tuozzi, and M. Belloni, in *2019 Joint Conference of the IEEE International Frequency Control Symposium and European Frequency and Time Forum (EFTF/IFC)* (IEEE, Orlando, FL, United States, 2019).

[25] C. E. Calosso, M. Gozzelino, A. Godone, H. Lin, F. Levi, and S. Micalizio, Intensity detection noise in pulsed vapor-cell frequency standards, IEEE Trans. Ultrason. Ferroelectr. Freq. Control **67**, 1074 (2020).

[26] C. E. Calosso, M. Gozzelino, E. Bertacco, S. Micalizio, B. François, and P. Yun, in *2017 Joint Conference of the European Frequency and Time Forum and IEEE International Frequency Control Symposium (EFTF/IFCS)* (IEEE, Besançon, France, 2017), p. 322.

[27] C. Cohen-Tannoudji and D. Guéry-Odelin, *Advances in Atomic Physics: An Overview* (World Scientific, Singapore, 2011).

[28] M. Arditi and J. L. Picqué, Precision measurements of light shifts induced by a narrow-band GaAs laser in the 0-0 ^{133}Cs hyperfine transition, J. Phys. B: At. Mol. Phys. **8**, L331 (1975).

[29] G. J. Dick, in *Proceedings of the 19th Annual Precise Time and Time Interval Systems and Applications Meeting* (Institute of Navigation, California, CA, United States, 1989), p. 133.

[30] L. Lo Presti, D. Rovera, and A. De Marchi, A simple analysis of the Dick effect in terms of phase noise spectral densities, IEEE Trans. Ultrason. Ferroelectr. Freq. Control **45**, 899 (1998).

[31] M. Gozzelino, S. Micalizio, C. E. Calosso, J. Belfi, A. Sapia, M. Gioia, and F. Levi, Realization of a pulsed optically pumped Rb clock with a frequency stability below 10^{-15}, Sci. Rep. **13**, 12974 (2023).

[32] C. E. Calosso, S. Micalizio, A. Godone, E. K. Bertacco, and F. Levi, Electronics for the pulsed rubidium clock: Design and characterization, IEEE Trans. Ultrason. Ferroelectr. Freq. Control **54**, 1731 (2007).

[33] C. Affolderbach, C. Andreeva, S. Cartaleva, T. Karaulanov, G. Mileti, and D. Slavov, Light-shift suppression in laser optically pumped vapour-cell atomic frequency standards, Appl. Phys. B **80**, 841 (2005).

[34] M. Gozzelino, S. Micalizio, F. Levi, A. Godone, and C. E. Calosso, Reducing cavity-pulling shift in Ramsey-operated compact clocks, IEEE Trans. Ultrason. Ferroelectr. Freq. Control **65**, 1294 (2018).

[35] M. Huang and J. Camparo, Laser frequency modulation and PM-to-AM noise conversion in atomic clocks, IEEE Trans. Ultrason. Ferroelectr. Freq. Control **71**, 222 (2024).

[36] E. Batori, C. Affolderbach, M. Pellaton, F. Gruet, M. Violetti, Y. Su, A. K. Skrivervik, and G. Mileti, μPOP clock: A microcell atomic clock based on a double-resonance Ramsey scheme, Phys. Rev. Appl. **18**, 054039 (2022).

[37] J. Kitching, Chip-scale atomic devices, Appl. Phys. Rev. **5**, 031302 (2018).

[38] M. Abdel Hafiz, C. Carlé, N. Passilly, J. M. Danet, C. E. Calosso, and R. Boudot, Light-shift mitigation in a microcell-based atomic clock with symmetric auto-balanced Ramsey spectroscopy, Appl. Phys. Lett. **120**, 064101 (2022).

[39] P. D. Schwindt, T. M. Hoang, Y.-Y. Jau, and R. Overstreet, in *2018 IEEE International Frequency Control Symposium (IFCS)* (IEEE, California, CA, United States, 2018).

[40] I. Manai, A. Molineri, C. Fréjaville, C. Duval, P. Bataille, R. Journet, F. Wiotte, B. Laburthe-Tolra, E. Maréchal, M. Cheneau, and M. R. de Saint-Vincent, Shelving spectroscopy of the strontium intercombination line, J. Phys. B: At., Mol. Opt. Phys. **53**, 085005 (2020).